Electrode potential dominates the reversibility of lithium metal anodes

Atsuo Yamada (yamada@chemsys.t.u-tokyo.ac.jp)
The University of Tokyo https://orcid.org/0000-0002-7880-5701
Seongjae Ko
The University of Tokyo
Tomohiro Obukata
The University of Tokyo
Tatau Shimada
The University of Tokyo
Norio Takenaka
The University of Tokyo https://orcid.org/0000-0001-7813-4736
Masanobu Nakayama
Nagoya Institute of Technology
Yuki Yamada
Osaka University https://orcid.org/0000-0002-7191-7129

Physical Sciences - Article

Keywords: Lithium metal batteries, plating/stripping, coordination, redox potential, machine learning

Posted Date: February 1st, 2022

DOI: https://doi.org/10.21203/rs.3.rs-1274809/v1

Version of Record: A version of this preprint was published at Nature Energy on October 27th, 2022. See the published version at https://doi.org/10.1038/s41560-022-01144-0.

Electrode potential dominates the reversibility of lithium metal anodes

Seongjae Ko[1,#], Tomohiro Obukata[1,#], Tatau Shimada[1], Norio Takenaka,[1] Masanobu Nakayama[2], Atsuo Yamada[1], Yuki Yamada[1,3*]*

1. Department of Chemical System Engineering, The University of Tokyo, 7-3-1, Hongo, Bunkyo-ku, Tokyo 113-8656, Japan
2. Department of Advanced Ceramics, Nagoya Institute of Technology, Showa-ku, Nagoya, Aichi 466-8555, Japan
3. SANKEN (The Institute of Scientific and Industrial Research), Osaka University, Mihogaoka 8-1, Ibaraki, Osaka 567-0047, Japan

# These authors equally contributed to this work.

Corresponding Author

*E-mail: Atsuo Yamada; yamada@chemsys.t.u-tokyo.ac.jp

*E-mail: Yuki Yamada; yamada@sanken.osaka-u.ac.jp

KEYWORDS: Lithium metal batteries, plating/stripping, coordination, redox potential, machine learning

Abstract

Li metal batteries are a promising technology for satisfying the emerging demands of high-energy-density storage systems. However, their pragmatic utilisation encounters a low Coulombic efficiency (CE) with the unceasing reductive decomposition of an electrolyte on Li metal with strong reducing ability. By improving the CE based on the chemistry of passivation films (i.e. solid electrolyte interphase, SEI), suppression of reductive decomposition has been achieved in a kinetic manner. However, the vague correlation between the CE and SEI has hampered further electrolyte development. Here, we report that in diverse electrolytes, the large shift (>0.6 V) in the Li electrode potential and its correlation with the Li^+ coordination state are 'hidden factors' that dominate the CE. Vibrational spectroscopy and machine learning hierarchal analysis revealed that the formation of ion pairs is essential for upshifting the Li electrode potential, that is, for weakening the reducing ability of Li, which would lead to a high CE with diminished electrolyte decomposition. Based on these criteria, various electrolytes enabling a significantly improved CE (>99%) were easily discovered. The findings of this study provide insights for the development of next-generation electrolytes for Li metal batteries.

Li metal is an ultimate anode for high-energy-density rechargeable batteries as it presents high theoretical capacity (3860 mAh g^{-1}) and low electrode potential (-3.04 V vs. standard hydrogen electrode).[1,2] However, its low plating/stripping Coulombic efficiency (CE) is the biggest barrier to their practical utilisation.[3,4] The low CE is attributed to the thermodynamic instability of a Li/organic electrolyte interface because of the strong reducing ability of Li.[3,4] The electrode potential of Li is located far outside the potential window of an organic electrolyte (Figure 1a), which induces the reductive decomposition of the electrolyte. In some cases, the reduction products are deposited on the Li surface, serving as a Li^+-conductive yet electron-insulating layer, referred to as the solid electrolyte interphase (SEI), which may effectively retard further electrolyte decomposition (i.e. kinetically extend the potential window).[5,6]

The nature of the SEI is an essential factor that dominates CE. To maximise the effect of SEIs, diverse electrolytes have been designed over the past decades. First, organic carbonates (e.g. propylene carbonate (PC) and ethylene carbonate (EC)) were applied as a solvents to form SEI, but the resulting CE (<90%) was far below the requirement (>99.9%).[7,8] Next, ether-based electrolytes (e.g. tetrahydrofuran (THF) and 1,2-dimethoxyethane (DME)) were developed, which exhibited high reduction stabilities, decreasing the gap between potential window and Li potential, leading to higher CE.[8,9] State-of-the-art electrolyte designs focus more on the stability of SEI; for example, concentrated electrolytes, locally concentrated electrolytes with non-polar solvents, and weakly solvating electrolytes form LiF-rich inorganic SEIs via preferential reductive decomposition of fluorinated salts or solvents, resulting in high electrochemical/mechanical stabilities and high CE ≥99%.[9–13] However, the correlation between the nature of SEI and CE is still unclear because the SEI is typically analysed via indirect experimental methodologies (e.g. ex situ morphology and chemistry analyses on damaged Li surfaces via pre-washing and/or pre-sputtering). Even in the presence of similar LiF-rich SEIs, there is considerable variation in CEs (90%–99%), depending on bulk electrolytes.[9,12–15] Hence, it is worth exploring another essential factor that dominates CEs.

Herein, we report the Li electrode potential (E_{Li}), defined as the inner potential difference between Li and the electrolyte, as a quantitative thermodynamic descriptor that dominates the CEs of Li anodes. This study focuses on the influence of E_{Li} on the CE because E_{Li} varies significantly depending on the electrolyte; specifically, E_{Li} is directly linked to the chemical potential of Li^+ (μ_{Li^+}) in the electrolyte.[16] Hence, E_{Li}, that is, the reducing ability of Li, can be controlled by designing an electrolyte with focus on μ_{Li^+}. If E_{Li} is strategically shifted upward (weakening the reducing ability of Li) to decrease the gap from the potential window, undesirable electrolyte decomposition can be diminished, which would considerably improve the CE of Li anodes (Figure 1a). This strategy has been implemented in a few studies: i) ultra-high CEs (≥99.9%) have been obtained for Na metal anodes with 0.3 V higher electrode potential,[17,18] and ii) highly reversible Li^+ intercalation of $Li_4Ti_5O_{12}$ has been achieved by increasing the electrode potential into the potential window in concentrated aqueous electrolytes.[19,20] In this study, we demonstrate that the shift of E_{Li} is considerably large (>0.6 V) depending on the organic electrolytes used, and higher E_{Li} leads to higher CEs of Li metal anodes. Furthermore, we identified characteristic local coordination structures and related spectroscopic features that strongly correlate with E_{Li}, which will facilitate the design of high-CE electrolytes for Li metal anodes.

We measured the E_{Li} in 74 different electrolytes. Ferrocene (Fc, at ~1 mM) was introduced into the electrolytes as an IUPAC-recommended internal standard for electrode potentials.[16,21,22] Assuming that the electrode potential of Fc/Fc^+ is constant and independent of the electrolytes[21,22], E_{Li} was measured with reference to Fc/Fc^+ on a Pt electrode (Figure 1b). Note that this cell does not contain any liquid junction, thus eliminating the effect of uncertain liquid junction potential.[23] Next, we applied the same 74 different electrolytes (without Fc) to Cu|Li cells to test the CEs of Li plating/stripping reactions on Cu. Li plating was conducted at a constant current density of 0.5 mA cm^{-2} for 1 h, followed by Li stripping at the same current density up to a cut-off voltage of 0.5 V. Average CE was calculated from the 2nd to 20th cycles of the three cells for each electrolyte. The 1st cycle was excluded because

it was primarily affected by the SEI formation process. To compare the data with a standard electrolyte for Li metal electrodes, E_{Li} (V vs. Fc/Fc^+) was also converted to E_{Li} (V vs. Li/Li^+ in 1 M LiFSI/DME (-3.40 V vs. Fc/Fc^+)).

The relationship between E_{Li} and the average CE of Li plating/stripping in 74 different electrolytes is presented in Figure 2. Clearly, the average CE increased with increasing E_{Li}, suggesting that the reductive decomposition of electrolytes was suppressed at high E_{Li} (lower reducing ability of Li). On this basis, it is essential to design an electrolyte with E_{Li} >-3.3 V vs. Fc/Fc^+, achieving high average CE >95%. Notably, even at the same E_{Li}, the CEs varied depending on the solvents used; ethers resulted in CEs >90% at -3.3 V vs. Fc/Fc^+, but sulfolane led to low CE of ~80%. This was attributed to the difference in the potential window of each solvent. Since ethers have wide potential windows in a reductive direction, the E_{Li} of -3.3 V vs. Fc/Fc^+ is sufficiently high to decrease the gap between E_{Li} and the potential windows.[9,12]

To more clearly demonstrate the effect of E_{Li} on CE, we picked up three ether electrolytes with similar potential windows: 1.5 M LiFSI/diglyme (G2), 1.5 M LiFSI/DME, and 1.5 M LiFSI/dimethoxymethane (DMM). These electrolytes have remarkably varying values of E_{Li}, -3.45 V, -3.38 V, and -3.16 V (vs. Fc/Fc^+), and hence, -0.05 V, 0.02 V, and 0.24 V (vs Li/Li^+ in 1 M LiFSI/DME), respectively (Figure 3b and S3), which are derived from the different solvation energies to Li^+ (discussed later). The CEs of the Cu|Li cells are shown in Figure 3c-e. In 1.5 M LiFSI/G2 with the lowest E_{Li} of -3.45 V vs. Fc/Fc^+ (-0.05 V vs. Li/Li^+ in 1 M LiFSI/DME), significant fluctuations of CEs were observed, suggesting the instability of plated Li with the electrolyte. In 1.5 M LiFSI/DME with slightly higher E_{Li} of -3.38 V vs. Fc/Fc^+ (0.02 V vs Li/Li^+ in 1 M LiFSI/DME), the fluctuation was still observed, but the CE was slightly improved. In striking contrast, in 1.5 M LiFSI/DMM with the highest E_{Li} of -3.16 V vs. Fc/Fc^+ (0.24 V vs Li/Li^+ in 1 M LiFSI/DME), highly stable Li

plating/stripping was observed, and the CE was remarkably improved up to 99.1% on average over 400 cycles.

These improved CEs have thus far been attributed to the nature of SEIs. In particular, LiFSI is believed to form good SEI. In this context, we analysed the surface of cycled Cu using X-ray photoelectron spectroscopy (XPS). As shown in Figure S4, LiFSI-derived components/moieties (LiF, S-N-S, Li-N, S=O, and sulfides) were observed for all three ether electrolytes.[24] Specifically, sulfides, which are reduced forms of LiFSI, were more abundantly observed for 1.5 M LiFSI/G2, which in turn showed poor CE.[24] Hence, SEI chemistries alone cannot account for the varied CEs in the three ether electrolytes. Because SEI can only kinetically suppress the reductive decomposition of the electrolyte, a considerably low E_{Li} (i.e. high reducing ability of Li) accelerates the decomposition reaction, leading to a low CE even in the presence of a similar SEI.

Another possible factor that influences CEs is the shape of the deposited Li. Generally, less dendritic deposition decreases the active surface area in contact with the electrolyte, leading to higher CEs. Scanning electron microscopy (SEM) images show that the morphologies of the deposited Li were similar in the three ether electrolytes (Figure S5). This suggests that the improved CE was not derived from the deposition morphology. Based on these observations, we concluded that E_{Li} influences the CE of Li metal anodes.

With a general theoretical background, we now discuss the dependence of E_{Li} on electrolytes. E_{Li} is determined by the chemical potential difference of the relevant species, as follows:

$$\mathrm{Li^+ + e^- \rightleftarrows Li} \qquad [1]$$

$$E_{\mathrm{Li}} = -\frac{1}{F}\left(\mu_{\mathrm{Li}}^{\mathrm{Li}} - \mu_{\mathrm{Li^+}} - \mu_{\mathrm{e}}^{\mathrm{Li}}\right) = \frac{\mu_{\mathrm{Li^+}}}{F} + \mathrm{const} \qquad [2]$$

where F, μ_{Li}^{Li}, μ_{Li^+}, and μ_e^{Li} correspond to the Faraday constant and the chemical potentials of Li (in Li metal), Li^+ (in electrolyte), and e^- (in Li metal), respectively. The second equal sign in equation (2) holds because μ_{Li}^{Li} and μ_e^{Li} are independent of the electrolyte used. On this basis, the observed variation in E_{Li} was derived from the different μ_{Li^+} values in the electrolytes.

Further, we discuss the determination of μ_{Li^+} . By definition, μ_{Li^+} is the molar Gibbs free energy change when an infinitesimal amount of Li^+ is added to an electrolyte solution. Because Li^+ exists bound to the solvent or counter anion, its coordination environment should dominate μ_{Li^+}, and hence, E_{Li}. To confirm this, machine learning hierarchal analysis of descriptors was conducted using partial least squares (PLS) regression and a computation-derived descriptor set, such as radial distribution function (RDF), composition, density, dipole moment, and highest occupied molecular orbital (HOMO)/lowest unoccupied molecular orbital (LUMO) values. The inset of Figure 4(a) displays diagnostic plots of regression results, showing good agreement between experimental and PLS-predicted E_{Li} for both validation and test data (root mean squared error, RMSE, ~0.05 V). Figure 4(a) presents the normalized prediction function coefficients (relative importance of descriptors) in descending order, indicating that the coordination environment around Li^+ (especially, the coordination to the FSI^- anion) is highly relevant for E_{Li}.

In this context, we analysed the coordination states of Li^+-FSI^- in various electrolytes using Raman spectroscopy. Figure 4(b) and 4(c) show the Raman spectra and their peak positions of the FSI^- anion, which represent Li^+-FSI^- ion-pairing states.[25] Notably, the Raman peak position is strongly correlated with E_{Li} in various electrolytes. E_{Li} increases as FSI^- is more extensively ion-paired with Li^+ from solvent-separated ion pairs (SSIPs; solvated Li^+ without FSI^- coordination) to contact ion pairs (CIPs; Li^+ coordinated with FSI^-) and aggregates (AGGs; aggregation of ion pairs).[25] This correlation agrees well with the machine learning-based prediction that the ion-pairing state of Li^+ dominates μ_{Li^+}, and thus E_{Li} as well.

The relationship between the coordination state, E_{Li}, and CE provides clear insights for developing rational electrolyte design strategies for Li metal batteries. As seen in Figures 2 and 4, the average CEs increased rapidly in the low-E_{Li} range (from -3.5 to -3.3 V vs. Fc/Fc^+, equivalent to approximately -0.1 V to 0.1 V vs. Li/Li^+ in LiFSI DME), wherein the coordination state began to be dominated by ion pairs (CIPs). This trend slowed but continued in the high-E_{Li} range (from -3.3 to -2.9 V vs. Fc/Fc^+, equivalent to 0.1 V to 0.5 V vs. Li/Li^+ in LiFSI DME), along with the coordination state transition from CIPs to AGGs. This hints that the electrolyte should be designed such that the anion is coordinated to Li^+ (at least in the state of CIPs) to achieve >95% CE.

The improved Li plating/stripping CEs obtained with state-of-the-art electrolytes (weakly solvating electrolytes, concentrated electrolytes, and locally concentrated electrolytes with non-polar solvents) can be reasonably and consistently explained based on their coordination states and E_{Li} (Figures 2 and 4). First, weakly solvating electrolytes promote the formation of CIPs and AGGs, thereby upshifting E_{Li} and increasing the CE. This trend is clearly observed in our model electrolytes, namely 1.5 M LiFSI/G2, 1.5 M LiFSI/DME, and 1.5 M LiFSI/DMM. The solvation energies were in the following order: G2 > DME > DMM (Figure S6). Notably, G2 is more strongly coordinated to Li^+ than DME owing to the substantial chelating effect of the three oxygen atoms.[26] Further, DMM shows the anomeric effect (Figure S6a), which thermodynamically favours a *gauche-gauche* conformation that cannot chelate Li^+; therefore, DMM is more weakly coordinated to Li^+ than DME.[27,28] The Raman peak of FSI^- was located at 718, 720, and 740 cm^{-1} for 1.5 M LiFSI/G2, 1.5 M LiFSI/DME, and 1.5 M LiFSI/DMM, respectively; moreover, the extent of ion pairing was in the order of G2 < DME < DMM (Figures 3). Importantly, such ion-pairing states are reflected by E_{Li} and the CE: The AGG-dominated 1.5 M LiFSI/DMM showed a 0.29 V higher E_{Li} (-3.16 V vs. Fc/Fc^+, which is 0.24 V vs. Li/Li^+ in 1 M LiFSI/DME) and higher CE than those of the SSIP-dominated 1.5 M LiFSI/G2 (-3.45 V vs. Fc/Fc^+, which is -0.05 V vs. Li/Li^+ in 1 M LiFSI/DME) (Figures 2, 3, and S1-S2).

Finally, this concept can be extended to concentrated electrolytes and locally concentrated electrolytes with non-polar solvents (e.g., highly fluorinated ethers (HFE) and toluene, which are inert toward Li^+ solvation), both of which have an effect similar to that of weakly solvating electrolytes. With an increasing salt concentration or upon introducing a non-polar solvent, the Raman peak of FSI^- gradually shifted from the lower-wave number range (~720 cm^{-1}; SSIPs) to the higher-wavenumber range (>730 cm^{-1}; CIPs and AGGs), which also increased E_{Li} and the CE (Figures 4(b), 4(c) and S1, S2, S7-S9). For instance, both the concentrated LiFSI/DME (1/1.4, n/n) (Figures S1 and S2) and locally concentrated 1.5 M LiFSI/DME:toluene (3.5:6.5, n:n) (Figure S9) with the ion-pair-dominated solution structure (Raman peak positions at 743 cm^{-1} and 732 cm^{-1}, respectively) exhibited an enhanced CE with an upshifted E_{Li} (-3.06 V and -3.18 V vs. Fc/Fc^+, which are 0.34 V and 0.22 V vs. Li/Li^+ in 1 M LiFSI/DME, respectively); specifically, these values were higher than those of 1.5 M LiFSI/DME (1/6.0, n/n) (-3.38 V vs. Fc/Fc^+, which is 0.02 V vs. Li/Li^+ in 1 M LiFSI/DME) with the SSIP-dominated solution structure (Raman peak position at 720 cm^{-1}). Thus far, the high CEs obtained using such state-of-the-art electrolytes have been discussed solely based on SEI chemistry; by contrast, the present work proposes the significant variations in E_{Li} (by over 0.6 V) as another contributing factor to the CEs.

In conclusion, the CE of Li plating/stripping was positively correlated with the thermodynamic electrode potential of Li metal (E_{Li}). An electrolyte with a high E_{Li}, thus weakening the reducing ability of Li metal, can minimise the reductive decomposition of the electrolyte, leading to a high CE. Machine-learning-based hierarchical analysis revealed that E_{Li} is substantially affected by Li^+–FSI^- interactions. Correspondingly, E_{Li} was strongly correlated with the Raman shift of FSI^-, which shows the extent of Li^+–FSI^- ion pairing. Importantly, we can predict E_{Li} from vibrational information. Based on these insights, highly reversible Li plating/stripping (>99%) was achieved with strongly ion-paired LiFSI/DMM and LiFSI/DME:toluene electrolytes owing to the anomeric effect and salt-concentration-localising effect by non-polar solvent, respectively. Moreover, this rationale is consistent with the high

CEs reported for other state-of-the-art electrolytes for Li metal batteries (e.g., weakly solvating electrolytes, concentrated electrolytes, and locally concentrated electrolytes). This paper does not refute the contribution of the SEI, which kinetically suppresses electrolyte decomposition; however, we determined a case in which CE was remarkably improved with increasing E_{Li}, even in the presence of similar SEIs. We believe that the thermodynamic metrics discovered here will provide new opportunities to design next-generation electrolytes for Li metal batteries.

References

1. Lin, D., Liu, Y. & Cui, Y. Reviving the lithium metal anode for high-energy batteries. *Nat. Nanotechnol.* **12**, 194–206 (2017).
2. Liu, B., Zhang, J.-G. & Xu, W. Advancing Lithium Metal Batteries. *Joule* **2**, 833–845 (2018).
3. Zhang, X., Yang, Y. & Zhou, Z. Towards practical lithium-metal anodes. *Chem. Soc. Rev.* **49**, 3040–3071 (2020).
4. Zhang, Y. *et al.* Towards better Li metal anodes: Challenges and strategies. *Mater. Today* **33**, 56–74 (2020).
5. Cheng, X.-B. *et al.* A Review of Solid Electrolyte Interphases on Lithium Metal Anode. *Adv. Sci.* **3**, 1500213 (2016).
6. Tikekar, M. D., Choudhury, S., Tu, Z. & Archer, L. A. Design principles for electrolytes and interfaces for stable lithium-metal batteries. *Nat. Energy* **1**, 16114 (2016).
7. Aurbach, D., Ein-Ely, Y. & Zaban, A. The Surface Chemistry of Lithium Electrodes in Alkyl Carbonate Solutions. *J. Electrochem. Soc.* **141**, L1–L3 (1994).
8. Ue, M. & Uosaki, K. Recent progress in liquid electrolytes for lithium metal batteries. *Curr. Opin. Electrochem.* **17**, 106–113 (2019).
9. Yu, Z. *et al.* Molecular design for electrolyte solvents enabling energy-dense and long-cycling lithium metal batteries. *Nat. Energy* **5**, 526–533 (2020).
10. Suo, L., Hu, Y.-S., Li, H., Armand, M. & Chen, L. A new class of Solvent-in-Salt electrolyte for high-energy rechargeable metallic lithium batteries. *Nat. Commun.* **4**, 1481 (2013).
11. Gao, X., Chen, Y., Johnson, L. & Bruce, P. G. Promoting solution phase discharge in Li-O2 batteries containing weakly solvating electrolyte solutions. *Nat. Mater.* **15**, 882–888 (2016).
12. Jiao, S. *et al.* Stable cycling of high-voltage lithium metal batteries in ether electrolytes. *Nat.*

Energy 1–8 (2018).
13. Fan, X. *et al.* Highly Fluorinated Interphases Enable High-Voltage Li-Metal Batteries. *Chem* **4**, 174–185 (2018).
14. Chen, M. *et al.* Marrying Ester Group with Lithium Salt: Cellulose-Acetate-Enabled LiF-Enriched Interface for Stable Lithium Metal Anodes. *Adv. Funct. Mater.* **31**, 1–10 (2021).
15. Ko, J. & Yoon, Y. S. Recent progress in LiF materials for safe lithium metal anode of rechargeable batteries: Is LiF the key to commercializing Li metal batteries? *Ceram. Int.* **45**, 30–49 (2019).
16. Mozhzhukhina, N. & Calvo, E. J. Perspective—The Correct Assessment of Standard Potentials of Reference Electrodes in Non-Aqueous Solution. *J. Electrochem. Soc.* **164**, A2295–A2297 (2017).
17. Seh, Z. W., Sun, J., Sun, Y. & Cui, Y. A Highly Reversible Room-Temperature Sodium Metal Anode. *ACS Cent. Sci.* **1**, 449–455 (2015).
18. Doi, K. *et al.* Reversible Sodium Metal Electrodes: Is Fluorine an Essential Interphasial Component? *Angew. Chemie Int. Ed.* **58**, 8024–8028 (2019).
19. Yamada, Y. *et al.* Hydrate-melt electrolytes for high-energy-density aqueous batteries. *Nat. Energy* **1**, (2016).
20. Ko, S. *et al.* Lithium-salt monohydrate melt: A stable electrolyte for aqueous lithium-ion batteries. *Electrochem. commun.* **104**, 106488 (2019).
21. Gagne, R. R., Koval, C. A. & Lisensky, G. C. Ferrocene as an internal standard for electrochemical measurements. *Inorg. Chem.* **19**, 2854–2855 (1980).
22. Gritzner, G. & Kůta, J. Recommendations on reporting electrode potentials in nonaqueous solvents. *Electrochim. Acta* **29**, 869–873 (1984).
23. Kim, S. C. *et al.* Potentiometric Measurement to Probe Solvation Energy and Its Correlation to Lithium Battery Cyclability. *J. Am. Chem. Soc.* **143**, 10301–10308 (2021).
24. Yamada, Y. *et al.* General Observation of Lithium Intercalation into Graphite in Ethylene-Carbonate-Free Superconcentrated Electrolytes. *ACS Appl. Mater. Interfaces* **6**, 10892–10899 (2014).
25. Han, S.-D., Borodin, O., Seo, D. M., Zhou, Z.-B. & Henderson, W. A. Electrolyte Solvation and Ionic Association. *J. Electrochem. Soc.* **161**, A2042–A2053 (2014).
26. Zhang, C. *et al.* Chelate Effects in Glyme/Lithium Bis(trifluoromethanesulfonyl)amide Solvate Ionic Liquids. I. Stability of Solvate Cations and Correlation with Electrolyte Properties. *J. Phys. Chem. B* **118**, 5144–5153 (2014).
27. Wiberg, K. B. & Murcko, M. A. Rotational barriers. 4. Dimethoxymethane. The anomeric effect

revisited. *J. Am. Chem. Soc.* **111**, 4821–4828 (1989).

28. Tvaroška, I. & Bleha, T. Lone pair interactions in dimethoxymethane and anomeric effect. *Can. J. Chem.* **57**, 424–435 (1979).

29. Wang, J., Wolf, R. M., Caldwell, J. W., Kollman, P. A. & Case, D. A. Development and testing of a general Amber force field. *J. Comput. Chem.* **25**, 1157–1174 (2004).

30. Nishihara, S. & Otani, M. Hybrid solvation models for bulk, interface, and membrane: Reference interaction site methods coupled with density functional theory. *Phys. Rev. B* **96**, 2–3 (2017).

31. Giannozzi, P. *et al.* QUANTUM ESPRESSO: A modular and open-source software project for quantum simulations of materials. *J. Phys. Condens. Matter* **21**, (2009).

32. Spiegelman, C. H., Bennett, J. F., Vannucci, M., McShane, M. J. & Coté, G. L. A transparent tool for seemingly difficult calibrations: The parallel calibration method. *Anal. Chem.* **72**, 135–140 (2000).

33. Marini, F., Roncaglioni, A. & Novič, M. Variable selection and interpretation in structure - Affinity correlation modeling of estrogen receptor binders. *J. Chem. Inf. Model.* **45**, 1507–1519 (2005).

34. Jalem, R., Aoyama, T., Nakayama, M. & Nogami, M. Multivariate method-assisted *ab initio* study of olivine-type $LiMXO_4$ (main group M^{2+}–X^{5+} and M^{3+}–X^{4+}) compositions as potential solid electrolytes. *Chem. Mater.* **24**, 1357-1364 (2012).

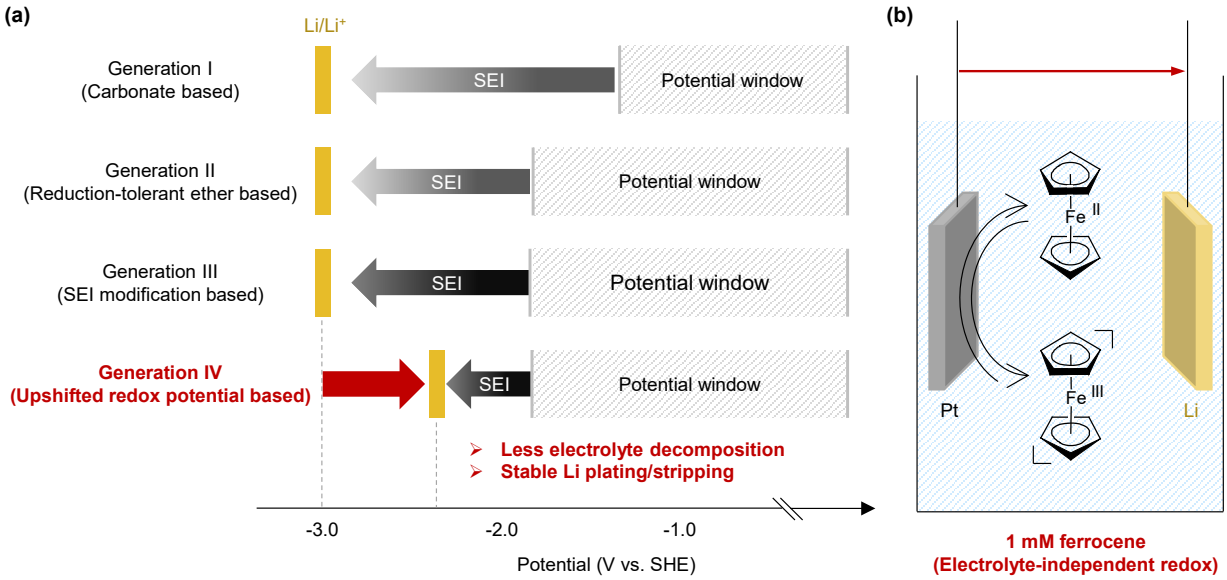

298

299 **Figure 1. Electrolyte design concept.** (a) History of electrolyte concepts for Li metal batteries. The
300 electrode potential of Li metal anodes is far from the potential window of non-aqueous electrolytes,
301 leading to a low CE accompanied by significant reductive decomposition of the electrolyte. Herein,
302 we aim to upshift the electrode potential of Li, thus weakening the reducing ability of Li, to suppress
303 the electrolyte decomposition. (b) Schematic of an electrochemical cell to measure the electrode
304 potential of Li in various electrolytes with reference to an IUPAC-recommended electrolyte-
305 independent redox species, ferrocene (Fc/Fc^+).[16,21,22]

306

307

308

309

310

311

312

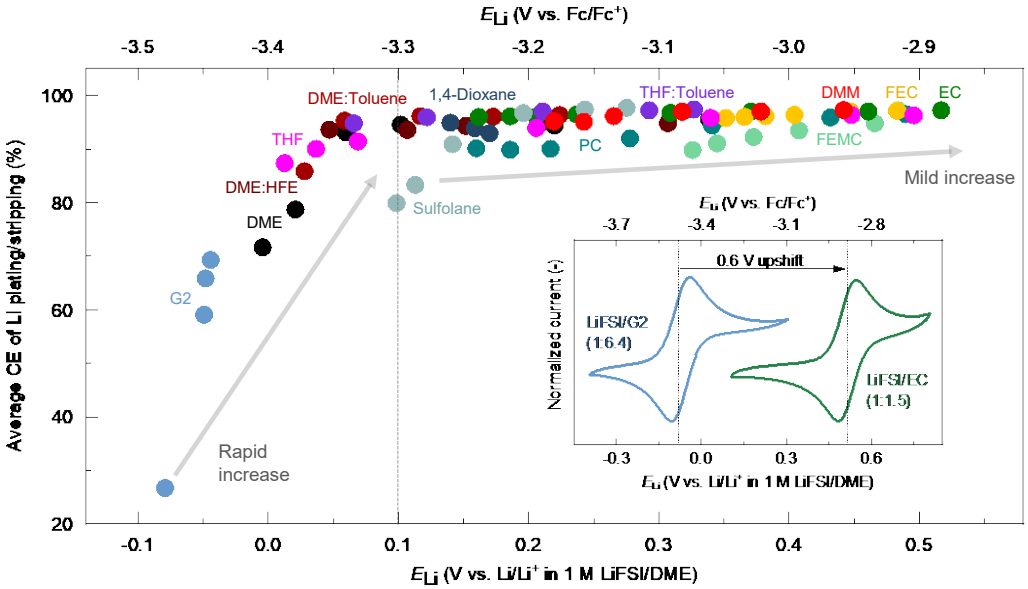

Figure 2. Coulombic efficiencies (CEs) of Li plating/stripping depending on the electrode potentials of Li (E_{Li}). High CEs were observed in electrolytes with high E_{Li}. Li | Cu cells were used for plating/stripping tests under identical conditions. The average CE was calculated from the second to the 20th cycle with three cells. Data for each electrolyte are shown in Figures S1 and S2. The inset represents cyclic voltammograms of ferrocene in the given electrolytes. The shift of E_{Li} (over 0.6 V), which determines the CEs of Li metal anodes, strongly depends on the electrolytes.

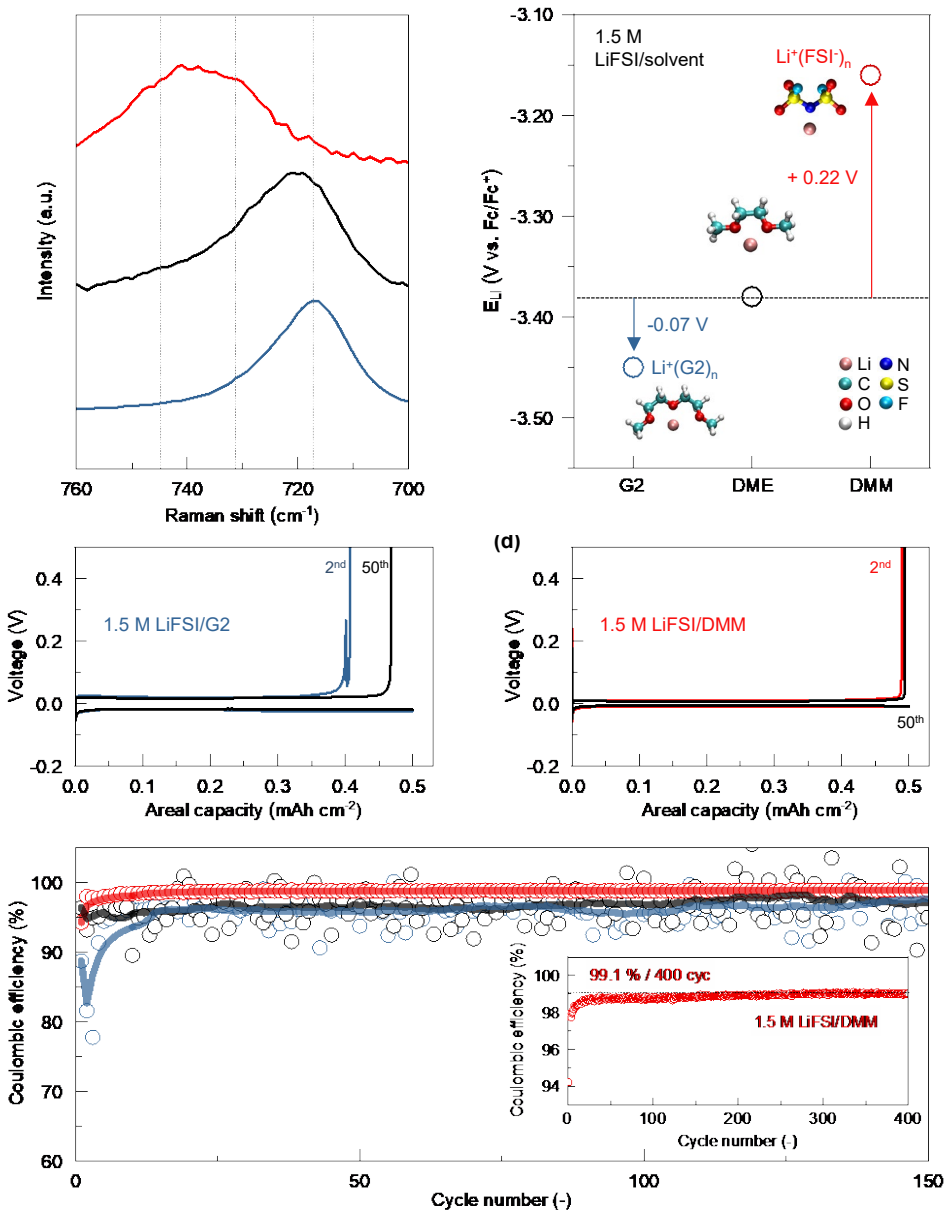

328

329 **Figure 3. Reversible Li plating/stripping enabled by electrode potential upshift in a weakly**
330 **coordinating solvent, DMM.** (a) Raman spectra of 1.5 M LiFSI/G2, 1.5 M LiFSI/DME, and 1.5 M
331 LiFSI/DMM. The peak position between 700 to 760 cm^{-1} represents the coordination condition of Li^+
332 and FSI^- ion pairs. (b) Electrode potential of Li (E_{Li}) with reference to Fc/Fc^+. (c),(d) Voltage curves
333 of Cu|Li cells with 1.5 M LiFSI/G2 and 1.5 M LiFSI/DMM electrolytes. (e) Coulombic efficiency of
334 Li plating/stripping reactions measured in Cu|Li cells with the aforenoted electrolytes. The solid lines
335 represent the smoothed curves obtained with 10-point adjacent averages. The long-term stability of Li
336 plating/stripping with 1.5 M LiFSI/DMM is shown in the inset. The upshifted redox potential of Li
337 metal in 1.5 M LiFSI/DMM, which is derived from the anomeric effect of DMM, enables a stable Li
338 plating/stripping reaction with a high Coulombic efficiency (~99.1%) over 400 cycles.

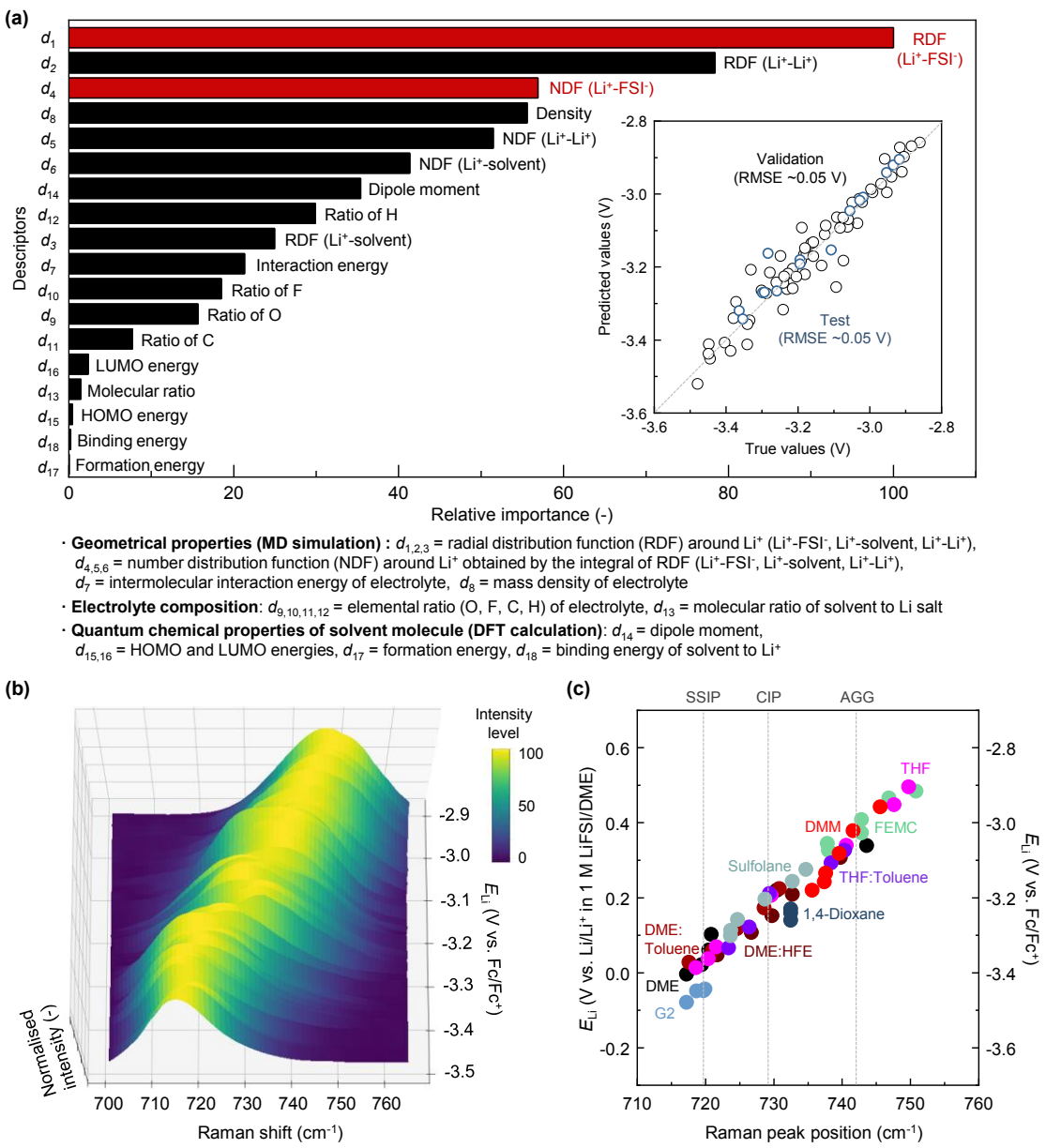

339

340 **Figure 4. Statistical and vibrational correlation between coordination states and the electrode**
341 **potentials of Li (E_{Li}).** (a) Normalised prediction function coefficients (relative importance of
342 descriptors) obtained from machine-learning-based PLS regression analysis for E_{Li}. The correlation
343 between the predicted and observed true values of E_{Li} is shown as an inset figure, along with the RMSE
344 values. The details of the descriptors (d_n) are provided at the bottom and in the methodology section.
345 The descriptors related to the coordination of FSI^- to Li^+ (red colour) are highly correlated with E_{Li}. (b)
346 Raman spectra of various electrolytes plotted in the order of their inherent E_{Li} values. The peak position
347 of FSI^- anion in the range of 700-760 cm^{-1} (ν_s(S-N-S)) represents the ion-pairing state of Li^+-FSI^-. (c)
348 E_{Li} of various electrolytes plotted against the Raman peak positions of FSI^- anion. The Raman spectra
349 of electrolytes composed of sulfolane, EC, PC, or FEC, which involve solvent-derived peaks at around

700-760 cm^{-1}, are demonstrated separately in Figure S8. Data for each electrolyte are shown in Figures S1, S2, S7, and S8.

Methodology section

Electrochemical study

The electrolytes were prepared by dissolving lithium bis(fluorosulfonyl)imide (LiFSI, $LiN(SO_2F)_2$, Nippon Shokubai) into the given solvents in an Ar-filled glove box. All the electrochemical tests were performed at room temperature. Cyclic voltammetry (CV) was conducted using a VMP3 potentiostat (BioLogic) to evaluate E_{Li} in a three-electrode cell consisting of a Pt working electrode and Li metal counter and reference electrodes with various electrolytes containing 1 mmol L^{-1} ferrocene (Fc, Sigma Aldrich). The redox potential of Fc/Fc^+ was measured with reference to Li/Li^+, and E_{Li} of various electrolytes was quantified assuming that the potential of Fc/Fc^+ is constant according to IUPAC recommendations.[16,21,22] Electrochemical Li plating/stripping tests were performed using half-cells (Cu|Li) with various electrolytes without Fc. The coin-cell parts (stainless-steel positive and negative cases, springs, spacers, and polypropylene O-rings) were purchased from Hoshen. A glass-fibre separator (GC50, Adventec) with a large pore size was selected to immerse electrolytes (Figure 2). In some experiments, a polypropylene (PP, Cellgard) membrane was used as an optimised separator to obtain long-term-cycling data (Figure 3). Note that the trend of the Coulombic efficiency based on the redox potential of Li in the various electrolytes did not change with different types of separators. Cu foil (Fuchikawa Rare Metal) and Li foil (Honjo Metal) were used without further treatment. The Li plating/stripping tests were conducted with a charge-discharge unit (TOSCAT-3100, Toyo System) at a constant current density of 0.5 mA cm^{-2} for 1 h during Li plating on Cu and up to a cut-off voltage of 0.5 V during Li stripping. The area of Li deposited on the Cu foil was 1.13 cm^2 (diameter = 1.2 cm). The average CE was calculated from the second to the 20th cycle

using three cells. The CE in the first cycle (SEI formation process) was excluded because we focused on the CE after SEI formation.

Materials characterisation

The liquid structure of the electrolytes was studied using Raman spectroscopy (NRS-5100 spectrometer, JASCO) with a laser excitation wavelength of 532 nm. The resolution of the Raman spectrometer was 0.8 cm^{-1}. To avoid air contamination, the electrolytes were sealed in quartz cells in an Ar-filled glove box, and the laser was irradiated through a quartz window. All the Raman peaks of the electrolytes were calibrated with a standard Si peak (520.7 cm^{-1}).

The surface morphology and chemical composition were evaluated using SEM (Hitachi S4800) and XPS (PHI5000 VersaProbe II, ULVAC-PHI) with a monochromatised Al Kα X-ray source. The cycled Cu electrodes in the given electrolytes were rinsed with DME several times in an Ar-filled glove box and transferred into the chambers without exposure to air by using a transfer vessel.

Computational study

Molecular dynamics (MD) simulations were performed to determine the geometrical properties of 74 different electrolytes. The atomic charges of all molecules and ions were obtained using gas-phase density functional theory (DFT) calculations at the B3LYP/cc-pvdz level, and the general AMBER force field[29] was employed as the Lennard–Jones (LJ) parameter. The time step was set to 1 fs using the SHAKE method, which constrains the bond distances between hydrogen atoms and heavy atoms. The sizes of the simulation cells were adjusted by NPT-MD simulations at 1 bar and 298 K. Then, using NVT-MD simulations (298 K), the systems were equilibrated for 1 ns, followed by 1 ns production runs. The quantum chemical properties of 10 different solvent molecules (EC, PC, FEC, FEMC, G2, DME, DMM, THF, 1,4-Dioxane, and sulfolane) were evaluated using gas-phase DFT

calculations at the B3LYP/cc-pvdz level. The Amber16 and Gaussian16 packages were used for MD simulations and DFT calculations, respectively.

In the solvation energy calculations (Figure S6), the structures of G2, DME, and DMM were optimised by using the 3D-RISM method.[30] To remove the excess charge in the system, the ESM-RISM method was used to calculate the solvation free energies of Li^+ in the 1.5 M LiFSI/G2, 1.5 M LiFSI/DME, and 1.5 M LiFSI/DMM electrolytes. The modified quantum ESPRESSO code[31]was used to perform 3D-RISM and ESM-RISM calculations using 40 × 40 × 40 $Å^3$ and 20 × 20 × 63.5 $Å^3$ unit cells, respectively; here, only the target molecule/ion was treated quantum mechanically using DFT, whereas the other molecules/ions were treated based on the implicit solvent model using the RISM method. The exchange correlation energies were calculated using the PBE generalised gradient approximation with the plane-wave basis set and ultrasoft pseudopotential scheme. The cut-off energies were set to 40 and 320 Ry for the wave functions and augmented charge, respectively. The Brillouin zone was sampled using only the Γ point. The molar ratio of molecules/ions in RISM was determined based on the experimental results for each electrolyte. For the RISM calculations, the same atomic charge and force field were used as in the MD simulations.

Machine learning analysis

A machine learning analysis using the PLS regression method[32–34] was conducted to estimate the dominant physical factor affecting the upshift of E_{Li}. The following were adopted as the descriptors (explanatory variables): $d_{1,2,3}$ = vectors derived from RDF around Li^+ (Li^+-FSI^-, Li^+-solvent, Li^+-Li^+), $d_{4,5,6}$ = vectors derived from the number distribution function (NDF) around Li^+ obtained by the integral of the RDF (Li^+-FSI^-, Li^+-solvent, Li^+-Li^+), d_7 = intermolecular interaction energy of the electrolyte (per atom), d_8 = mass density of the electrolyte, $d_{9,10,11,12}$ = elemental ratio (O, F, C, H) of the electrolyte, d_{13} = molecular ratio of the solvent to Li salt, d_{14} = dipole moment of the solvent, $d_{15,16}$ = energies of the HOMO and LUMO of the solvent, d_{17} = formation energy of the solvent, and d_{18} =

binding energy of the solvent to Li^+. The geometrical ($d_{1\text{-}8}$) and quantum chemical properties ($d_{14\text{-}18}$) were obtained by MD simulations and DFT calculations, respectively. Further, 80% of the dataset was randomly selected and used for training/validation, while test predictions were performed on the remaining 20%. A 10-partition cross-validation method was adopted and seven latent variables were used in this study. The importance of $d_{1\text{-}6}$ was given as the maximum value among those in each bin (0.5 Å interval) of the RDF and NDF.

Acknowledgements

This work was supported by the Advanced Low Carbon Technology Research and Development Program (ALCA), Specially Promoted Research for Innovative Next Generation Batteries (SPRING) of the Japan Science and Technology Agency (JST) (JPMJAL1301) to Y.Y., JSPS KAKENHI Specially Promoted Research (No. 15H05701) to A.Y., and the Ministry of Education, Culture, Sports, Science, and Technology (MEXT) Program: Data Creation and Utilization Type Materials Research and Development Project (JPMXP1121467561) to A.Y..

Author contributions

Y.Y. and A.Y. conceived and directed the projects. T.O., S.K., and Y.Y. proposed the concepts of the electrolyte design and electrode potential control. A.Y., N.T., and M.N. proposed the strategy and direction of the machine learning approach. S.K. and T.O. performed the experiments and analysed the data. T.S., N.T., and M.N. performed the computational and machine learning analyses. S.K., N.T., M.N., Y.Y., and A.Y. wrote the manuscript.

Competing interests

The authors declare no competing interests.

Supplementary Files

This is a list of supplementary files associated with this preprint. Click to download.

- supportinginformation.docx